Classical analogue of the ionic Hubbard model

M. Hafez,[1] S. A. Jafari,[2,3,*] Sh. Adibi,[2] and F. Shahbazi[2]

[1]*Department of Physics, Tarbiat Modares University, Tehran, Iran*
[2]*Department of Physics, Isfahan University of Technology, Isfahan 84156-83111, Iran*
[3]*School of Physics, Institute for Research in Fundamental Sciences (IPM), Tehran 19395-5531, Iran*

In our earlier work [M. Hafez *et al.*, Phys. Lett. A **373**, 4479 (2009)] we employed the flow equation method to obtain a classical effective model from a quantum mechanical parent Hamiltonian called, the ionic Hubbard model. The classical ionic Hubbard model (CIHM) obtained in this way contains solely Fermionic occupation numbers of two species corresponding to particles with ↑ and ↓ spin, respectively. In this paper, we employ the transfer matrix method to analytically solve the CIHM at finite temperature in one dimension. In the limit of zero temperature, we find two insulating phases at large and small Coulomb interaction strength, U, mediated with a gapless phase, resulting in two continuous metal-insulator transitions. Our results are further supported with Monte Carlo simulations.

I. INTRODUCTION

To understand the magnetism and magnetic phenomena, one of the basic interactions is the exchange mechanism, which is deeply associated with Coulomb interactions and quantum mechanical indistinguishability. Therefore a fair understanding of the magnetic behavior of materials is not possible without investigating appropriate quantum spin models. Introducing uniaxial anisotropy to the Heisenberg model amounts to suppression of transverse quantum fluctuations $(S^+S^- + S^-S^+)$, leading to the so called Ising model.[1] The resulting Ising Hamiltonian turns out to contain the basic magnetic phases of the original Heisenberg model, namely ferromagnetism, and antiferromagnetism.[2] However, many of the interesting aspects such as spin liquid phases, spin-wave excitations, etc.[3] cannot be captured by the Ising model. Classical Ising model has the merit of being much simpler to solve, and admits analytical[1,4] and graphical solutions[2] in various geometries[5] in one and two dimensions which is lacking in the original quantum Heisenberg model.

In addition to magnetic properties, dielectric properties are also important aspects characterizing materials. The question can be asked here, is there any Ising-like model that can provide "basic informations" about the phases of dielectric materials, and at the same time being simple enough to allow for analytical solutions? We have taken the example of the IHM.[6,7] This model was introduced to study the neutral-to-ionic transition in organic compounds and to understand the role of strong electronic correlations in the dielectric properties of metal oxides.[7,8] This model is given by:

$$H = -t\sum_{i\sigma}(c_{i\sigma}^\dagger c_{i+1,\sigma} + \text{H.c.}) + U\sum_i c_{i\uparrow}^\dagger c_{i\downarrow}^\dagger c_{i\downarrow} c_{i\uparrow}$$
$$+ \frac{\Delta}{2}\sum_{i\sigma}(-1)^i c_{i\sigma}^\dagger c_{i\sigma}, \qquad (1)$$

where $c_{i\sigma}(c_{i\sigma}^\dagger)$ is the usual annihilation (creation) operator at site i with spin σ. U is the on-site Coulomb interaction parameter, and Δ denotes a one-body staggered ionic potential.

The kinetic energy scale is given by the real hopping amplitude t which prefers to gain kinetic energy by spreading the wave function over the whole system, leading to quantum fluctuation of the charge density. The zero temperature phase diagram of this model contains Mott and band insulating states when the energy scales corresponding to U or Δ dominate, respectively.[8] When these two scales become comparable, the nature of intermediate phase still remains controversial. Some authors argue that the intermediate state is a spontaneously broken symmetry phase,[9–11] while some others argue that the phase in between is metallic.[6,8,12,13] In our previous investigation[8] we employed the method of flow equations for the quantum Hamiltonian Eq. (1) to obtain an effective Hamiltonian in which the hopping t term is renormalized to zero, producing a nearest-neighbor Coulomb attraction.

In continuous unitary transformation (CUT) method, the Hamiltonian can be transformed by a series of infinitesimal unitary transformation (parameterized by a flow parameter ℓ). Hamiltonian at $\ell=0$, corresponds to the initial Hamiltonian, and in the $\ell\to\infty$ one expects to recast the Hamiltonian into the (block) diagonalized form. This method can be formulated in terms of flow equations for various parameters of the Hamiltonian which is derived from the following equation:

$$\partial_\ell H(\ell) = [\eta(\ell), H(\ell)], \qquad (2)$$

where $\eta(\ell)$ is the so called *generator* of the flow. There are various possible choices for the generator. One possible choice is the generator suggested by Wegner:

$$\eta(\ell) = [H^d(\ell), H^r(\ell)], \qquad (3)$$

where $H^d(\ell)$ [$H^r(\ell)$] is diagonal (off-diagonal) part of the Hamiltonian. Choosing the Hubbard plus ionic terms as H^d, and subject to initial conditions at $\ell=0$: $t(0)=1$, $\Delta(0)=\Delta$, $U(0)=U$, and $V(0)=0$, where V is a nearest neighbor Coulomb interaction (induced during the flow process) we find

that ionic Hubbard model (IHM) Hamiltonian flows toward the following lattice gas form:

$$\tilde{H} = \frac{\tilde{\Delta}}{2}\sum_{i\sigma}(-1)^i n_{i\sigma} + \tilde{U}\sum_i n_{i\uparrow}n_{i\downarrow} + \tilde{V}\sum_{i\sigma,\sigma'} n_{i\sigma}n_{i+1\sigma'}, \quad (4)$$

where the renormalized parameters $\tilde{\Delta}$, $\tilde{U}$, $\tilde{V}$ denote the corresponding parameters in $\ell \to \infty$ limit, and have closed form expressions in terms of the bare parameters U, Δ.[8] We take the initial hopping energy scale $t(0)=t$ as the unit of energy. Flow of the above Hamiltonian is restricted to the two-particle sector, and we have ignored three-particle, and higher terms. In our calculations, we have used a generator which is first order in t. Therefore the resulting effective Hamiltonian misses the kinetic exchange (second order it t), and hence magnetic phases such as antiferromagnetic or spin density wave states cannot be captured with the effective lattice gas model Eq. (4).

By calculating the spin and charge gaps, we showed that this simple classical model is capable of capturing the physics of a gapless state sandwiched between two distinct insulating phases at zero temperature as a function of U for a fixed value of Δ.[8] Here, $n_{i\sigma}$ contains two species (or colors) corresponding to $\sigma=\uparrow,\downarrow$, respectively. Since n_σ for each "color" σ is either 0 or 1, it is an Ising-like variable. Therefore our effective CIHM Hamiltonian can be thought of, as two interpenetrating Ising models on a lattice. Being a natural extension of two species lattice gas model, allows for analytical solution in one spatial dimensions (1D). Here we can employ the transfer matrix method, constructed in terms of 3×3 matrices to calculate the thermodynamic properties of this model at finite temperatures. At high temperatures where the thermal fluctuations wash out the quantum effects, we expect the results of our calculations to be a good description of the class of materials modeled in terms of IHM. In 1D and at low temperatures where quantum fluctuations

play dominant role, the results obtained for effective Hamiltonian Eq. (4) will have little to do with the original quantum model. In these limits, it is interesting to study Eq. (4) as a lattice gas model on its own. Also a novel graphical solution in two dimensions (2D) similar to Feynman's construction can be worked out.[14]

The paper is organized as follows: In the next section, we calculate the grand canonical potential for this model in one dimension and discuss the particle density and ionicity in various fillings. It is followed by a section focused on half-filling situation, and calculate the specific heat, compressibility and ionicity to assess the nature of the phases in the parameter space of U, T. Throughout the paper we have fixed the value of $\Delta=20$.[8] The final section is devoted to summary and discussion.

II. GRAND POTENTIAL

In this section, we calculate the grand canonical potential that can be derived from the grand partition function (GPF) which is defined as follows:

$$Z(T,\mu,L) = \sum_{\{n_{i\sigma}\}} e^{-\beta\{E[(n_{i\sigma})]-\mu N[(n_{i\sigma})]\}}, \quad (5)$$

where T is Temperature, L is lattice size, and μ is chemical potential. $\{n_{i\sigma}\}$ denotes all possible configurations of the occupation numbers, which must be summed over. $N(\{n_{i\sigma}\})=\Sigma_{i\sigma}n_{i\sigma}$ is the number of particle and $E(\{n_{i\sigma}\})$ is the energy that is defined by the model Hamiltonian Eq. (4).

The summation in Eq. (5) can be calculated analytically as follows: Values of $n_{i\sigma}$ are only zero and one, which is the Fermionic memory left in the commuting variables $n_{i\sigma}$. Hence $n_{i\sigma}^2=n_{i\sigma}$, and the second term in Eq. (4) becomes,

$$\sum_i n_{i\uparrow}n_{i\downarrow} = \frac{1}{2}\sum_i (n_{i\uparrow}+n_{i\downarrow})[(n_{i\uparrow}+n_{i\downarrow})-1]. \quad (6)$$

Therefore GPF becomes,

$$Z(T,\mu,L) = \sum_{\{n_{i\sigma}\}}\exp\left\{-\beta\left[\sum_{i\sigma}\left((-1)^i\frac{\tilde{\Delta}}{2}-\mu\right)n_{i\sigma} + \frac{\tilde{U}}{2}\sum_{i\sigma,\beta}n_{i\sigma}\left(n_{i\beta}-\frac{1}{2}\right) + \tilde{V}\sum_{i\sigma,\beta}n_{i\sigma}n_{i+1\beta}\right]\right\}. \quad (7)$$

As can be seen at the Hamiltonian level, only the spin-summed occupation numbers appear and therefore this classical model unlike the quantum IHM does not contain spin-polarized (magnetic) solutions even in the $\Delta=0$ limit. So we change the summation variable from $n_{i\uparrow}$ and $n_{i\downarrow}$ to $n_i=n_{i\uparrow}+n_{i\downarrow}$ that has three possible values 0,1,2. Therefore we have:

$$Z = \sum_{\{n_i\}}\exp\left\{-\beta\sum_i\left[\left((-1)^i\frac{\tilde{\Delta}}{2}-\mu\right)n_i + \frac{\tilde{U}}{2}n_i(n_i-1) + \tilde{V}n_i n_{i+1}\right]\right\}\prod_{i=1}^{L}(1+\delta_{n_i,1}), \quad (8)$$

where the coefficient $\Pi_{i=1}^L(1+\delta_{n_i,1})$ takes into account the twofold degeneracy for $n_i=1$ in Eq. (7), which corresponds to either $n_{i\uparrow}=1$, $n_{i\downarrow}=0$, or $n_{i\uparrow}=0$, $n_{i\downarrow}=1$. Equation (8) can be written in a more symmetric form,

$$Z = \sum_{\{n_i\}}\prod_{i=1}^{L}(1+\delta_{n_i,1})^{1/2}(1+\delta_{n_{i+1},1})^{1/2}\exp\left\{-\beta\left\{+(-1)^i\frac{\tilde{\Delta}}{4}(n_i-n_{i+1}) - \frac{\mu}{2}(n_i+n_{i+1}) + \frac{\tilde{U}}{4}[n_i(n_i-1)+n_{i+1}(n_{i+1}-1)] + \tilde{V}n_i n_{i+1}\right\}\right\}, \quad (9)$$

where L is assumed to be even and the periodic boundary conditions, $n_{L+1}=n_1$ is implied. Defining the matrix elements of the transfer matrix M_{n_1,n_2} by,

$$M_{n_1,n_2} \equiv (1 + \delta_{n_1,1})^{1/2}(1 + \delta_{n_2,1})^{1/2}\exp\left\{ -\beta\left\{ +\frac{\tilde{\Delta}}{4}(n_1 - n_2) - \frac{\mu}{2}(n_1 + n_2) + \frac{\tilde{U}}{4}[n_1(n_1 - 1) + n_2(n_2 - 1)] + \tilde{V}n_1 n_2 \right\}\right\}, \quad (10)$$

Equation (9) can be written as:

$$Z = \sum_{n_1=0}^{2} \cdots \sum_{n_L=0}^{2} M_{n_2,n_1} M_{n_2,n_3} \cdots M_{n_L,n_{L-1}} M_{n_L,n_1}$$

$$= \sum_{n_1=0}^{2} \cdots \sum_{n_L=0}^{2} M^t_{n_1,n_2} M_{n_2,n_3} \cdots M^t_{n_{L-1},n_L} M_{n_L,n_1} = \mathrm{Tr}(M^t M)^{L/2}$$

$$(11)$$

where M^t is the transpose of M, $M_{n_2,n_1} \equiv (M^t)_{n_1,n_2}$. Then the partition can be written as,

$$Z = \lambda_1^{L/2} + \lambda_2^{L/2} + \lambda_3^{L/2}, \quad (12)$$

where λ_1, λ_2, and λ_3 are the eigenvalues of $M^t M$. In the thermodynamic limit where L is very large, the grand potential per site is,

$$\phi = -\frac{T}{2}\ln \lambda_{\max}. \quad (13)$$

Here $\lambda_{\max}$ is the maximum eigenvalue. Hence, to obtain the grand potential one needs to calculate the eigenvalues of $M^t M$. Later on, when we discuss the ionicity, in addition we will need the eigenvectors of $M^t M$ too. Eigenvalues of $M^t M$ are solutions to the third-order equation,

$$\lambda^3 + a_2\lambda^2 + a_1\lambda + a_0 = 0, \quad (14)$$

where a_2, a_1, and a_0 given in the appendix. Throughout this paper, we will report the numerical plots for $\Delta = 20$ in units in which $t(\ell = 0) = 1$. For this value of Δ, there would be no level crossing among the eigenvalues λ of the matrix $M^t M$ when one varies μ, T, and U, as expected from Perron's theorem.[15]

From the partition function, one can in principle calculate various averages of the form $\langle n_{i\sigma}n_{j\sigma'}\ldots\rangle$. The simplest of these averages are the average particle density $n \equiv \langle n_{2i+1} + n_{2i}\rangle/2$ (symmetric combination), and the ionicity $I \equiv \langle n_{2i+1} - n_{2i}\rangle/2$ (antisymmetric combination), which contain important information about the nature of the thermodynamic phases of the model. In the following, we calculate these averages as a function of μ.

A. Particle density

Once the grand potential ϕ is known, one can derive many other thermodynamic quantities. Particle density, n, can be calculated as,

$$n = -\left.\frac{\partial \phi}{\partial \mu}\right|_T. \quad (15)$$

In Fig. 1, particle density versus μ has been plotted for different values of T. In this figure the value of U is fixed to

be $U = 10$. This value of U mimics a band insulating regime at zero temperature.[8] As can be seen in the figure, apart from trivial cases of the empty ($n = 0$) and the completely filled ($n = 2$) lattice, there are three plateaus. The first one corresponds to the half-filling $n = 1$ (i.e., one particle per lattice site), and two others correspond to commensurate fillings, $n = 0.5$ (quarter filling), $n = 1.5$ (three-quarter filling) which is quite similar to the plateaus of the parent ionic Hubbard model.[12] Indeed the $n = 0.5$ and $n = 1.5$ are related by a particle-hole transformation. Therefore in what follows, we focus on $n = 0.5$, 1. With increasing the temperature, plateaus get more and more rounded. The value of chemical potential corresponding to the half-filling is independent of temperature, as can be seen in Fig. 1. The inset plot indicates this point more transparently. This "isosbestic" behavior is observed for all values of values of $10 < U < 40$.

In Fig. 2, we have plotted the particle density as a function of chemical potential μ at a constant (low) temperature $T = 0.4$, for different values of U. As can be seen in the figure, increasing U, causes the $n = 0.5$, 1.5 plateaus which are particle-hole counterpart of each other, to get wider. However the plateau at $n = 1.0$ gets narrower and finally vanishes around $U = 20$, resulting in a gapless phase at half-filling. Upon further increasing U, the half-filling plateau is recovered, and gets wider, indicating the emergence of a growing new gap in the system, which is reminiscent of the Mott
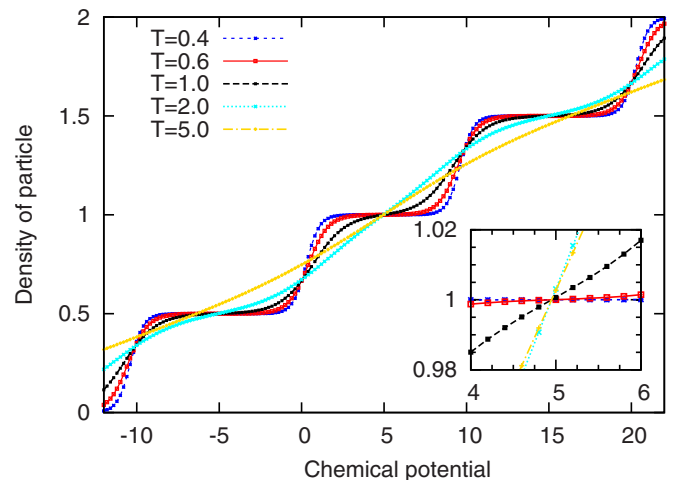

FIG. 1. (Color online) Particle density n, versus chemical potential μ for $U = 10$, $\Delta = 20$ and different temperatures. Three plateaus at $n = 0.5$, 1, and 1.5 correspond to quarter-, half-, and three quarter-fillings. For lower temperature, the variations of the density as a function of μ is very slow over the plateaus, which is clear signature of a gap in the spectrum at these commensurate fillings. By increasing the temperature, plateaus get rounder, which indicate the thermal energy starts to overcome the gaps. The inset magnifies the "isosbestic" behavior at $n = 1$ plateau.
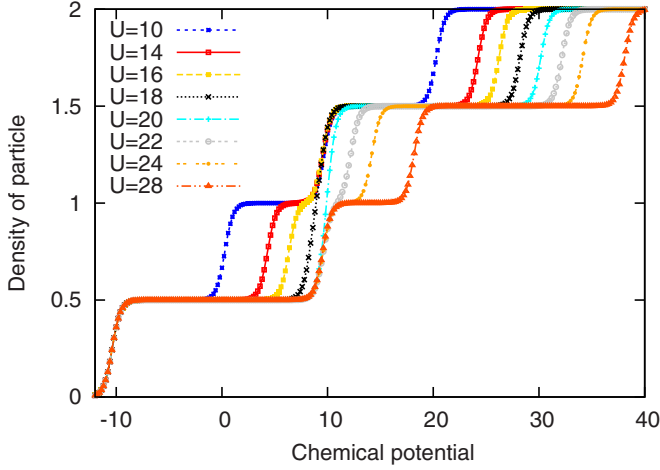
FIG. 2. (Color online) Particle density n, versus chemical potential μ for constant $T=0.4$, $\Delta=20$ and different values of U. As can be seen in general again there are three plateaus corresponding to $n=0.5$, 1, and 1.5. However, for intermediate values of U, the plateau at half-filling has disappeared.

insulating behavior. To identify the nature of gap at $n=0.5$, 1.5 one needs to calculate the ionicity, which provides information about how the unit cell is being filled. This will be done in the sequel.

For later reference, we report the value of chemical potential corresponding to half-filling, which by examining the numerical plots turns out to be:

$$\mu(T,U,n=1) = 0.495U, \tag{16}$$

which is very close to the value $U/2$ expected from symmetry considerations. The temperature range at which the above relation is valid, is roughly $0.1 \lesssim T$. For temperatures outside this range, there will be deviations from the above rule of thumb relation.

B. Ionicity

If A, B denote the sublattice of odd and even sites, respectively, then the populations N_A and N_B are defined as:

$$N_A = \sum_{i \in \text{odd}} \langle n_i \rangle, \tag{17}$$

$$N_B = \sum_{i \in \text{even}} \langle n_i \rangle. \tag{18}$$

The ionicity per site becomes $I=(N_A-N_B)/L$, where $n_i=n_{i\uparrow}+n_{i\downarrow}$, and L is the total number of lattice sites. This quantity can also be calculated analytically with the aid of transfer matrices. In the grand canonical ensemble $\langle n_j \rangle$ is given by:

$$\langle n_j \rangle = \frac{1}{Z}\sum_{\{n_{i\sigma}\}} n_j e^{-\beta\{E[(n_{i\sigma})]-\mu N[(n_{i\sigma})]\}}. \tag{19}$$

Depending on whether j is odd or even, similar to calculations for grand partition function, we obtain:

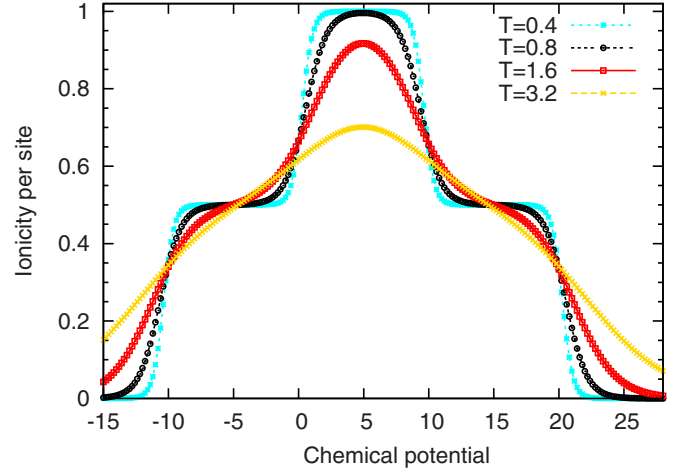$$\langle n_j \rangle = \frac{1}{Z}\text{Tr}[N(M^tM)^{L/2}], \text{for odd } j \tag{20}$$

FIG. 3. (Color online) The ionicity per site as a function of chemical potential for various temperatures at $U=10$. Three plateaus around $\mu \approx -5$, 5, 15 correspond to 1/4, 1/2, and 3/4 filling.

$$= \frac{1}{Z}\text{Tr}[N(MM^t)^{L/2}], \text{for even } j \tag{21}$$

where N is the following 3×3 matrix:

$$N_{n_1,n_2} = n_1 \delta_{n_1,n_2}. \tag{22}$$

In Fig. 3, we have plotted the ionicity per site as a function of μ for various temperatures at a fixed value of $U=10$. For this value of U, and in the IHM at zero temperature one would expect a band insulator at half-filling, where A-sublattice (with on-site energy $-\Delta/2$) are doubly occupied. Let us focus around $\mu=-5$ which corresponds to quarter filling (c.f. Figure 1). The value of $I=0.5$ for $\mu \approx -5$ in Fig. 3 shows that the only electron of each unit cell belongs to A-sublattice, which represents a charge density wave insulator.

As we increase μ from ≈ -5, the ionicity increases, which indicates that sublattice A continues to be filled. When $\mu \approx 5$, one approaches the half-filling (Fig. 1), where at lower temperatures the A-sublattice is totally occupied, hence $I \approx 1$. As can be seen in Fig. 3, this saturation value is decreased as the temperature is increased. This reduction in the ionicity, indicates that the particles are getting thermally excited across the band gap. Further increasing of the chemical potential, one reaches the plateau around $\mu \approx 15$ of Fig. 3 (c.f. Figure 1). The decrease in the ionicity indicates that the added particles essentially start to occupy B sublattice. The symmetry of Fig. 3 around $n=1$, is due to the apparent particle-hole symmetry of the Hamiltonian.

In Fig. 4, we plot the ionicity per site at the constant temperature $T=0.4$, for various values of U indicated in the legend. Again there are three plateaus corresponding to 1/4, 1/2 and 3/4-filling, respectively. This figure indicates that the center of the half-filling plateau is at $\mu_{\text{half}}=U/2$. This can be understood as a Hartree-like energy for the Hubbard model. Now concentrating around half-filling in this figure, for small values of U, the ionicity reaches 1, which indicates a complete electric polarization of the unit cell, and hence it mim-
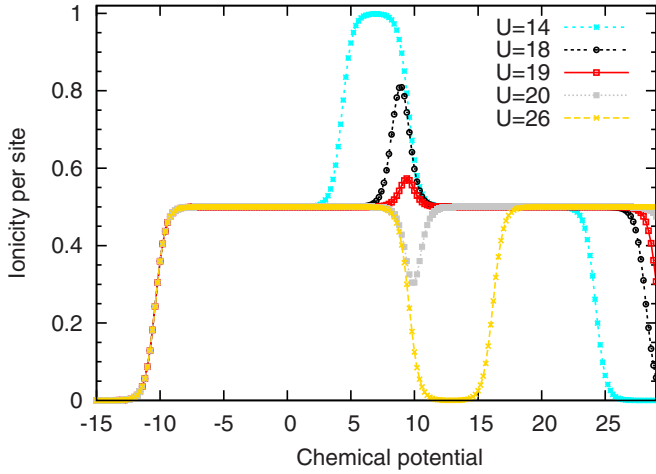
FIG. 4. (Color online) Ionicity per site as a function of μ and constant temperature $T=0.4$, for various values of U. Three plateaus correspond to 1/4, 1/2, and 3/4 filling, respectively. Note that the center of the half-filling plateau is at $\mu=U/2$.

ics a band insulator. For intermediate values of U, the maximum value of ionicity does not reach 1, which shows some of the added particles start to occupy the B sublattice. Also note that for the intermediate values of U the half-filling plateau starts to disappear, i.e., the emergence of a gap-less behavior. For large values of U, the half-filling plateau is restored, but at zero ionicity. Therefore the classical ground state resembles an insulator with unpolarized unit cell. Such an insulating state in our lattice gas model can be thought of as classical counterpart of the Mott insulating state. Note that Eq. (4) being a classical model, cannot describe a true quantum mechanical Mott insulating state, as it does not contain superexchange physics which is of second order in t.

III. HALF-FILLING

As we saw in Fig. 2, for $n=0.5$, 105 the U, Δ energy scales cooperate with each other, to give rise to a charge density wave insulating ground state. Rather at $n=1.0$, these two energy scales compete against each other to destroy the insulating behavior for intermediate U ($\sim\Delta$), giving rise to a richer phase diagram. Therefore in this section we focus at half-filling and calculate the specific heat, compressibility, and ionicity. Before doing so, we compare some physical quantities evaluated by a fully numerical Monte Carlo simulation, with our exact transfer matrix results. In Fig. 5, ionicity and specific heat per site are plotted at half-filling and show a good agreement between analytical and numerical results. This ensures us that both Monte Carlo and transfer matrix results are reliable.

Now let us proceed with the calculation of various thermodynamic quantities. For the fixed value of $\Delta=20$, we have two ways to plot thermodynamic quantities. First choice is to plot them as a function of temperature T, at some selected values of U. These results indicate that in the present one-dimensional model, there will be no finite temperature phase transition. This is obviously due to the analytic behavior of the partition function as a function of T. The second possi-
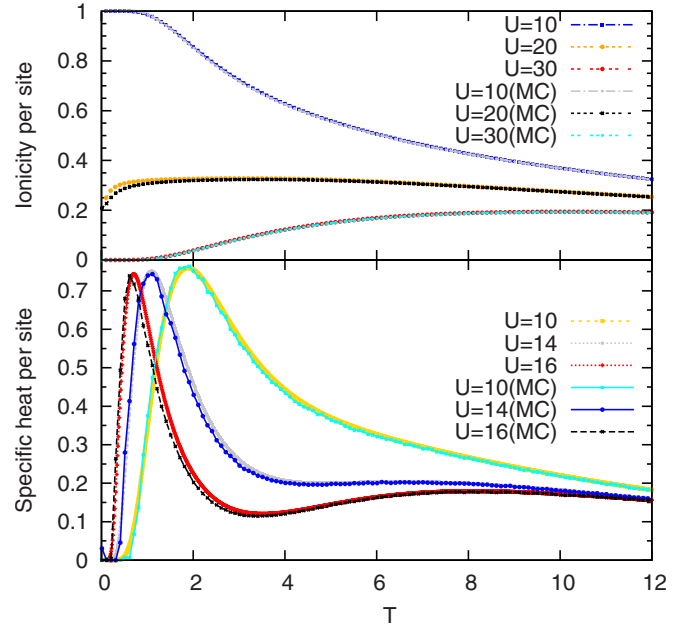

FIG. 5. (Color online) Ionicity and specific heat per site at half-filling from transfer matrix and Monte Carlo (MC) methods. To stay in the range of validity of Eq. (16), transfer matrix results are plotted for $T\gtrsim0.1$. Monte Carlo results are obtained for $L=500$ sites. As stated earlier, we are working at constant $\Delta=20$.

bility is to plot them as a function of U, for some selected temperatures. This second way of presenting the data, reveals that as one lowers the temperature, there will be sharper features as a function of U, indicating the zero temperature phase transition in this model which are reminiscent of the quantum phase transitions in the original IHM. Our calculations are based on Eqs. (13) and (16). For very low temperatures, where the validity of Eq. (16), might be questioned, we employ Monte Carlo simulation data.

A. Specific heat

Specific heat per site can be calculated as:

$$c_L = T\frac{\partial s}{\partial T}, \qquad (23)$$

where s is entropy per site at half-filling that can be derived from the grand potential. Figure 6 shows the specific heat versus T for various values of U. As can be seen in Fig. 6 for values of $U\leq14$, there is a single peak in the c_L. For $14 < U < 38$ a peak-dip-hump structure can be observed. For $U > 20$ the hump is quite clear, while for $U < 20$, it can be interpreted as a precursor to the hump. For $38 \leq U$, the peak merges into the hump structure. In terms of the parent quantum Hamiltonian, such hump structure corresponds to incoherent excitations. For $U=20$, Eq. (16) is not reliable at very low temperatures. Therefore, we report Monte Carlo simulation results which indicates a very sharp peak at $T\approx0$. As U moves toward ≈20 from both sides (lower and upper panels), the peak gets sharper and moves toward lower temperatures. This indicates that in $T\rightarrow0$ limit one expects a transition between gapped and gapless states. This behavior can be
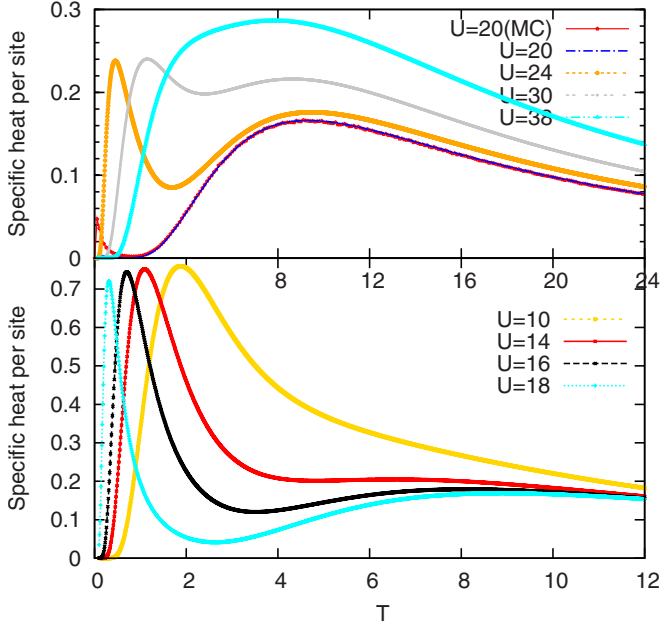
FIG. 6. (Color online) Specific heat per site versus T at $\Delta = 20$ for different values of U. For small values of U there is a single peak, which becomes a peak-dip- hump in intermediate U, and finally the peak merges into the hump at large U. For $U = 20$, both analytic and Monte Carlo results are reported. MC results are for $L = 500$ sites.

simply understood in terms of a two-state model with level spacing δ, whose specific heat is given by,

$$c_L = k_B \left[x^2 \frac{e^x}{(1 + e^x)^2} \right], \tag{24}$$

where $x = \delta / (k_B T)$. Behavior of Eq. (24) for $x \gg 1$ is like $\sim x^2 e^{-x}$, while for $x \ll 1$ it vanishes as $\sim x^2$. For the intermediate region a Schottky peak around $x_{peak} \sim 1$ ($\delta \sim k_B T$) arises in the specific heat. Fitting specific data to Eq. (24), we estimate gap magnitudes which has been plotted versus U in Fig. 7, and indicates two gapped phases. According to the
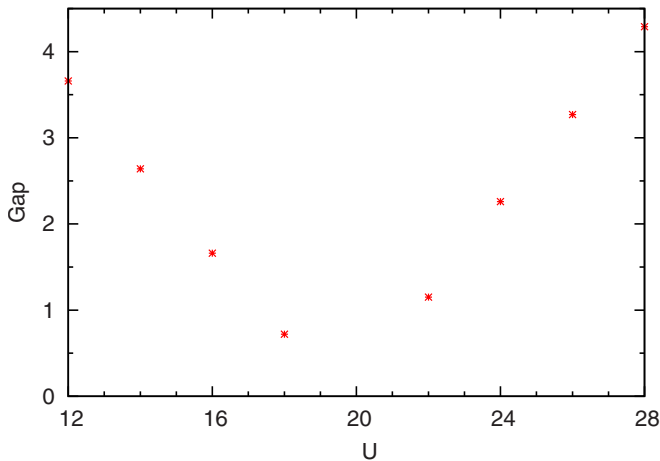

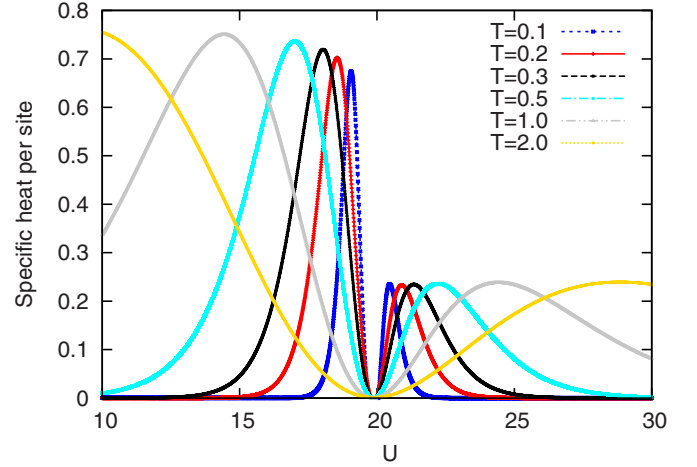FIG. 7. (Color online) Estimate of gap using two-state model as a function of U at $\Delta = 20$.

FIG. 8. (Color online) Specific heat per site versus U for different values of T.

above two-state formula, this peak corresponds to $\delta / k_B T \sim 1$, from which a gap of $\delta \sim 10^{-2}$ can be estimated. If we extrapolate the estimated gap for $18 < U < 22$, zero gap region is expected to occur for $U_{c_1} = 19.30 \lesssim U \lesssim U_{c_2} = 19.75$ which is compatible with our previous work.[8]

Now let us look at the specific heat data from a different angle. In Fig. 8, we plot the specific heat versus U for different values of temperatures. As can be seen, there are two peak structures at all temperatures, which get sharper and by lowering the temperature, they tend to accumulate around $U \approx 20$. Extrapolating the trend of this double-peak structure to the limit of $T \to 0$, suggests two phase transitions at U_{c1} and U_{c2},[8] compatible with the behavior of the vanishing gap region in Fig. 7. The characteristic quadratic behavior around $U \approx 20$ seen in Fig. 8, which according to the two-state model is expected to be like $c_L \propto (\delta / T)^2$, indicates two continuous metal-insulator transitions, with $\delta \sim |U - U_{c_i}|$, $i = 1, 2$

B. Compressibility

Another useful quantity that can be studied for CIHM is the compressibility which is given by:

$$\kappa = \frac{1}{n^2} \left. \frac{\partial n}{\partial \mu} \right|_T, \tag{25}$$

where $n = N / L$ is the density of particles per site.

In Fig. 9, we plot the compressibility as a function of T for different values of U. Zero compressibility is a characteristic of gapped states. As can be seen in this figure for small value of U the range of temperatures at which the compressibility is close to zero is substantial, which means that the gap is so large that up to such temperature the insulating behavior is still manifest. By increasing U, this temperature range shrinks and becomes smaller and smaller, until around $U = 20$, it extrapolates to zero. Increasing U beyond 20, again recovers a finite temperature range in which the compressibility is zero. This behavior confirms that a gap-less state is sandwiched between two gapped states.

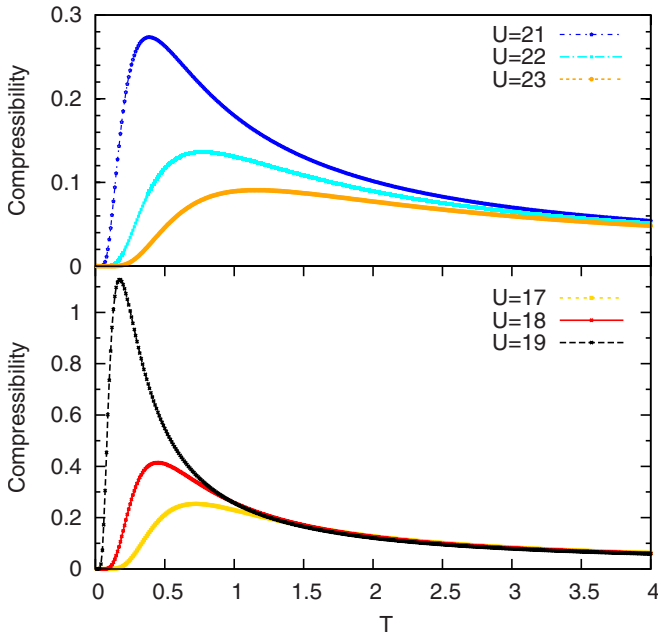To see the above statement more clearly, in Fig. 10, we plot compressibility as a function of U for selected tempera-

FIG. 9. (Color online) Compressibility versus T for different values of U.

tures. As can be seen in this figure, there is a region with nonzero compressibility which characterizes a gapless phase. Outside this region, the compressibility decays to zero. By decreasing T, the width of the compressibility peak becomes smaller while the height of the peak diverges as $T \rightarrow 0$; which is a typical characteristic of a continuous phase transition. This indicates the existence of a gapless phase at zero temperature for the CIHM.[8] The effect of thermal fluctuations is to smear the edges of gapless region. This is quite intuitive, as for values of U near the zero temperature boundary of gapless phase with neighboring insulating phases, the gaps are small, and hence the thermal energy can overcome the gap.

C. Ionicity

In Fig. 11, we plot the ionicity per site for $\Delta = 20$ and various values of U at half-filling. As can be seen in the
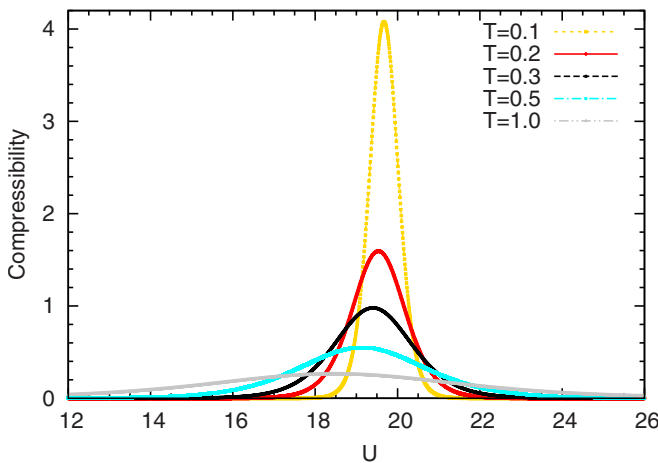

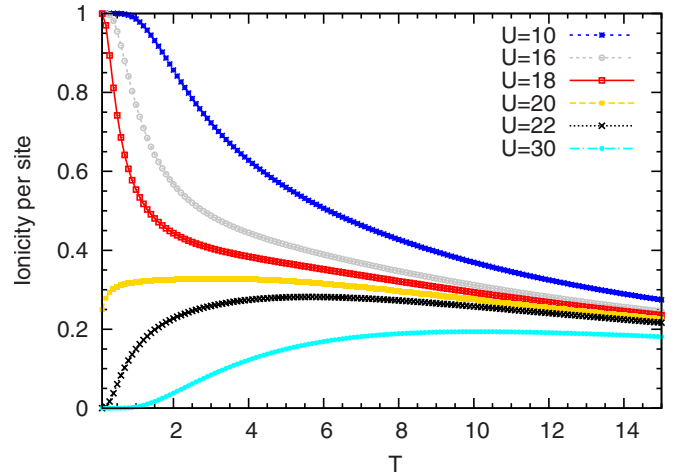FIG. 10. (Color online) Compressibility versus U for different values of temperature.

FIG. 11. (Color online) Ionicity versus T for $\Delta = 20$ and different values of U at half-filling.

figure, by lowering the temperature, for $U \leq 18$, the ionicity tends to $I = 1$; for $U > 20$ it reaches a zero temperature value of $I = 0$; while for $U \approx 20$, it reaches a value between these two limits; characterizing a phase with charge fluctuations.

This behavior can be understood as follows: At small U regime the unit cell is fully polarized at low temperatures, with both ↑ and ↓ particles occupying the A sublattice. As the temperature is increased, some of the particles get excited to B sublattice by absorbing the thermal energy, $k_B T$. On the other hand, for large values of U, at lower temperatures the unit cell is not polarized, due to the Coulomb term U. By increasing the temperature, thermal excitations with doubly occupied sites will be created, thereby increasing the ionicity. For intermediate $U \approx 20$, the weights of polarized and unpolarized configurations in the unit cell become comparable; hence giving the ionicity $0 < I < 1$.

In Fig. 12, we plot the ionicity at half-filling as a function of U for $\Delta = 20$ and various values of T. As can be seen at all temperatures, the ionicity smoothly varies between 1 for small values U, and 0 for large values of U. The width of the transition region decreases by lowering the temperature, and is expected to approach the Fig. 2 of Ref. 8.
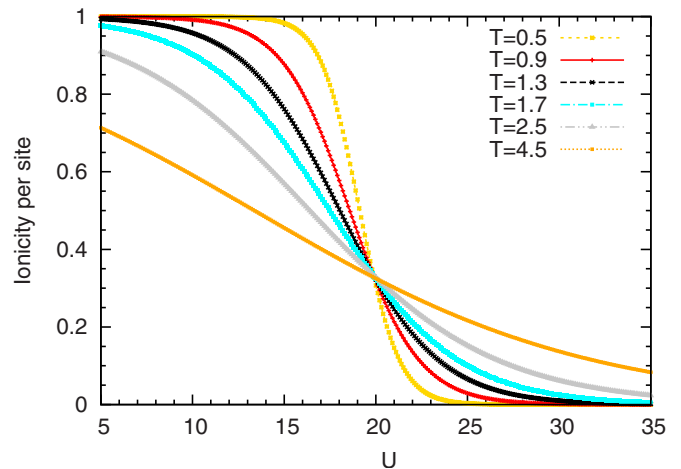

FIG. 12. (Color online) Ionicity versus U for some values of temperature at half-filling and $\Delta = 20$.

IV. CONCLUSION

In this work, we studied a classical model consisting of two Ising-like variables on a one dimensional chain. Despite the simplicity which essentially results from the lack of Fermionic minus sign problem, our model captures some of the interesting properties of the ionic Hubbard model. However, since in our model Eq. (4), quantum fluctuations are not present, at low temperatures and low dimensions one has to be careful about attributing the results obtained for classical model Eq. (4) to the original quantum IHM.

Various thermodynamic properties of CIHM, such as specific heat, ionicity, particle density and compressibility when viewed as a function of U in a given temperature, indicate the presence of two gapped states at small and large values of U, with a gap-less state sandwiched between them (around $U/\Delta \approx 1$). When the same quantities are viewed as a function of temperature, there is no sign of phase transition down to zero temperature. The sharp zero temperature phase transitions at $U_{c_1}(\Delta)$ and $U_{c_2}(\Delta)$, turn into crossover, due to thermal smearing of phase boundaries.

Mapping of D dimensional quantum models to $D+1$ dimensional classical Hamiltonians is a well known paradigm in statistical physics. Our flow equation approach[8] suggests an alternative approach to construct "D" dimensional classical models which might be useful in capturing some basic aspects of the original quantum Hamiltonian at finite temperatures.

ACKNOWLEDGMENTS

APPENDIX

Coefficients of Eq. (14)

The coefficients a_2, a_1, and a_0 of Eq. (14) are as follows:

$$a_2 \equiv -\{e^{-\beta(2\tilde{\Delta}+2\mu+\tilde{U})} + 2e^{-3/2\beta(\tilde{\Delta}+2\mu)} + e^{-\beta(4\mu+\tilde{\Delta})}$$
$$+ 2e^{-1/2\beta(3\tilde{\Delta}+2\mu+2\tilde{U}+8\tilde{V})} + 4e^{-\beta(\tilde{\Delta}+2\mu+2\tilde{V})} + 2e^{-1/2\beta(\tilde{\Delta}+6\mu)}$$
$$+ e^{-\beta(2\tilde{U}+8\tilde{V}+\tilde{\Delta})} + e^{-\beta(\tilde{U}+2\mu)} + 2e^{-1/2\beta(2\tilde{U}+8\tilde{V}+2\mu+\tilde{\Delta})}\}e^{\beta(4\mu+\tilde{\Delta})}, \tag{A1}$$

$$a_1 \equiv -\{-4e^{-\beta(2\tilde{\Delta}+2\mu+\tilde{U}+2\tilde{V})} + 4e^{-1/2\beta(4\tilde{U}+12\tilde{V}+2\mu+\tilde{\Delta})}$$
$$- 4e^{-\beta(2\tilde{U}+10\tilde{V}+\tilde{\Delta})} - 2e^{-1/2\beta(4\tilde{U}+16\tilde{V}+3\tilde{\Delta}+2\mu)}$$
$$- e^{-\beta(2\tilde{U}+8\tilde{V}+2\mu+\tilde{\Delta})} + 4e^{-1/2\beta(2\tilde{U}+4\tilde{V}+\tilde{\Delta}+6\mu)} - e^{-\beta(2\tilde{U}+\tilde{\Delta}+2\mu)}$$
$$+ 4e^{-1/2\beta(4\tilde{U}+12\tilde{V}+3\tilde{\Delta}+2\mu)} + 4e^{-1/2\beta(2\tilde{U}+3\tilde{\Delta}+6\mu+4\tilde{V})}$$
$$- 2e^{-1/2\beta(\tilde{\Delta}+6\mu+2\tilde{U})} + 8e^{-\beta(2\tilde{\Delta}+2\mu+\tilde{U}+3\tilde{V})} + 8e^{-\beta(4\mu+\tilde{\Delta}+\tilde{V})}$$
$$- 4e^{-\beta(4\mu+\tilde{\Delta})} - 4e^{-\beta(2\tilde{U}+8\tilde{V}+\tilde{\Delta})} - 2e^{-1/2\beta(4\tilde{U}+3\tilde{\Delta}+8\tilde{V}+2\mu)}$$
$$+ 8e^{-\beta(2\tilde{U}+9\tilde{V}+\tilde{\Delta})} - 2e^{-1/2\beta(4\tilde{U}+8\tilde{V}+\tilde{\Delta}+2\mu)} + 2e^{-\beta(2\tilde{U}+4\tilde{V}+\tilde{\Delta}+2\mu)}$$
$$- 4e^{-\beta(2\tilde{\Delta}+2\mu+\tilde{U}+4\tilde{V})} - 4e^{-\beta(\tilde{U}+2\tilde{V}+2\mu)}$$
$$- 2e^{-1/2\beta(2\tilde{U}+3\tilde{\Delta}+6\mu+8\tilde{V})} - 2e^{-1/2\beta(4\tilde{U}+16\tilde{V}+2\mu+\tilde{\Delta})}$$
$$- 2e^{-1/2\beta(2\tilde{U}+6\mu+8\tilde{V}+\tilde{\Delta})} - 2e^{-1/2\beta(2\tilde{U}+3\tilde{\Delta}+6\mu)} - 4e^{-\beta(4\mu+\tilde{\Delta}+2\tilde{V})}$$
$$+ 8e^{-\beta(\tilde{U}+3\tilde{V}+2\mu)} - 4e^{-\beta(\tilde{U}+4\tilde{V}+2\mu)}\}e^{\beta(\tilde{\Delta}+6\mu)}, \tag{A2}$$

$$a_0 \equiv 4e^{-2\beta(\tilde{U}+\tilde{V}-3\mu)}\{-4e^{-2\beta\tilde{V}} - 4e^{-5\beta\tilde{V}} - 4e^{-3\beta\tilde{V}} + 10e^{-4\beta\tilde{V}}$$
$$+ 4e^{-\beta\tilde{V}} + 4e^{-7\beta\tilde{V}} - 4e^{-6\beta\tilde{V}} - e^{-8\beta\tilde{V}} - 1\}. \tag{A3}$$

*akbar.jafari@gmail.com

[1] G. F. Newell and E. W. Montroll, Rev. Mod. Phys. **25**, 353 (1953).

[2] R. P. Feynman, *Statistical Mechanics* (Westview Press, Reading, MA, 1998).

[3] E. Fradkin, *Field Theories of Condensed Matter Systems* (Westview Press, Reading, MA, 1998).

[4] L. Onsager, Phys. Rev. **65**, 117 (1944).

[5] S. A. Jafari, Int. J. Mod. Phys. B **23**, 395 (2009).

[6] N. Nagaosa and J. Takimoto, J. Phys. Soc. Jpn. **55**, 2735 (1986).

[7] T. Egami S. Ishihara, and M. Tachiki Science **261**, 1307 (1993).

[8] M. Hafez, S. A. Jafari, and M. R. Abolhassani, Phys. Lett. A **373**, 4479 (2009).

[9] M. Fabrizio, A. O. Gogolin, and A. A. Nersesyan, Phys. Rev. Lett. **83**, 2014 (1999); C. D. Batista and A. A. Aligia, *ibid.* **92**, 246405 (2004); S. R. Manmana, V. Meden, R. M. Noack, and K. Schönhammer, Phys. Rev. B **70**, 155115 (2004); Ö. Legeza, K. Buchta, and J. Sólyom, *ibid.* **73**, 165124 (2006); T. Wilkens and R. M. Martin, *ibid.* **63**, 235108 (2001); S. S. Kancharla and E. Dagotto, Phys. Rev. Lett. **98**, 016402 (2007).

[10] L. Tincani, R. M. Noack, and D. Baeriswyl, Phys. Rev. B **79**, 165109 (2009).

[11] Ö. Legeza and J. Sólyom, Phys. Rev. Lett. **96**, 116401 (2006).

[12] K. Bouadim, N. Paris, F. Hébert, G. G. Batrouni, and R. T. Scalettar, Phys. Rev. B **76**, 085112 (2007).

[13] A. Garg, H. R. Krishnamurthy, and M. Randeria, Phys. Rev. Lett. **97**, 046403 (2006); N. Gidopoulos, S. Sorella, and E. Tosatti, Eur. Phys. J. B **14**, 217 (2000); N. Paris, K. Bouadim, F. Hébert, G. G. Batrouni, and R. T. Scalettar, Phys. Rev. Lett. **98**, 046403 (2007).

[14] S. A. Jafari and F. Shahbazi (unpublished).

[15] N. Goldenfeld, *Lecture on Phase Transitions and The Renormalization Group* (Westview Press, Reading, MA, 1992).